arXiv:0912.5083v2 [nlin.CD] 5 Feb 2010

Ulam method and fractal Weyl law for Perron–Frobenius operators

L.Ermann and D.L.Shepelyansky

1 Laboratoire de Physique Théorique (IRSAMC), Université de Toulouse, UPS, F-31062 Toulouse, France
2 LPT (IRSAMC), CNRS, F-31062 Toulouse, France
3 http://www.quantware.ups-tlse.fr

February 4, 2010

Abstract. We use the Ulam method to study spectral properties of the Perron-Frobenius operators of dynamical maps in a chaotic regime. For maps with absorption we show that the spectrum is characterized by the fractal Weyl law recently established for nonunitary operators describing poles of quantum chaotic scattering with the Weyl exponent $\nu = d - 1$, where d is the fractal dimension of corresponding strange set of trajectories nonescaping in future times. In contrast, for dissipative maps we find the Weyl exponent $\nu = d/2$ where d is the fractal dimension of strange attractor. The Weyl exponent can be also expressed via the relation $\nu = d_0/2$ where d_0 is the fractal dimension of the invariant sets. We also discuss the properties of eigenvalues and eigenvectors of such operators characterized by the fractal Weyl law.

1 Introduction

The Weyl law gives a fundamental relation between a number of quantum states in a given classical phase space volume and an effective Planck constant $\hbar$ for Hermitian operators [1]. Recently, this relation has been extended to nonunitary quantum operators which describe complex spectrum of open systems or poles of scattering problem. In this case the fractal Weyl law determines a number of Gamow eigenstates in a complex plane of eigenvalues with finite decay rates γ via a fractal dimension d of a classical fractal set of nonescaping orbits. The Gamow eigenstates find applications in various types of physical problems including decay of radioactive nuclei [2], quantum chemistry reactions [3], chaotic scattering [4] and chaotic microlasers [5]. It is interesting that the fractal Weyl law was first introduced by mathematicians via rigorous mathematical bounds [6]. Later, numerical simulations for systems with quantum chaotic scattering and open quantum maps confirmed the mathematical bounds and determined a number of interesting properties of such nonunitary quantum operators [7,8,9,10,11]. Open quantum maps with absorption, e.g. the Chirikov standard map [12], are very convenient for numerical studies that allowed to establish a number of intriguing properties of decay rates and quantum fractal eigenstates in the limit of large matrix size and small scale quantum resolution [13,10].

The fractal Weyl law gives the following scaling for the number of Gamow states N_γ with the decay rate in a finite band width $0 \le \gamma \le \gamma_b$:

$$N_\gamma \propto N^\nu , \quad N = V/\hbar , \quad \nu = d - 1 , \qquad (1)$$

where N is a matrix size given by a number of quantum states in a volume V and the exponent ν is determined by a fractal dimension d of classical set formed by classical trajectories nonescaping in future times (see Fig.1).

In view of the result (1) it is natural to assume that the fractal Weyl law should also work for other type of nonunitary matrix operators. An important type of such matrices is generated by the Ulam method [14] applied to the Perron-Frobenius operators of dynamical systems [15]. The method is based on discretization of the phase space and construction of a Markov chain based on probability transitions between such discrete cells given by the dynamics. It is proven that for hyperbolic maps in one and higher dimensions the Ulam method converges to the spectrum of continuous system [16]. While the spectrum of such Ulam matrix approximant of continuous operator has been studied numerically for various dynamical maps (see e.g [17] and Refs. therein) the validity of the fractal Weyl law has not been investigated. Mathematical results for the Selberg zeta function [19] indicate that the law (1) should remain valid but, as we show here, for certain dynamical systems the exponent ν starts to depend on fractal dimension d in a different way.

It is known that in certain cases the Ulam method gives significant modifications of the spectrum compared to the case of the continuous Perron-Frobenius operators [16]. In fact discretization by phase-space cells effectively introduces small noise added to dynamical equations of motion. For Hamiltonian systems with divided phase space this noise destroys the invariant curves and drastically changes the eigenstate of the Perron-Frobenius operator (see e.g. discussion in [18]). However, for homogeneously chaotic systems the effect of this noise is rather weak com-
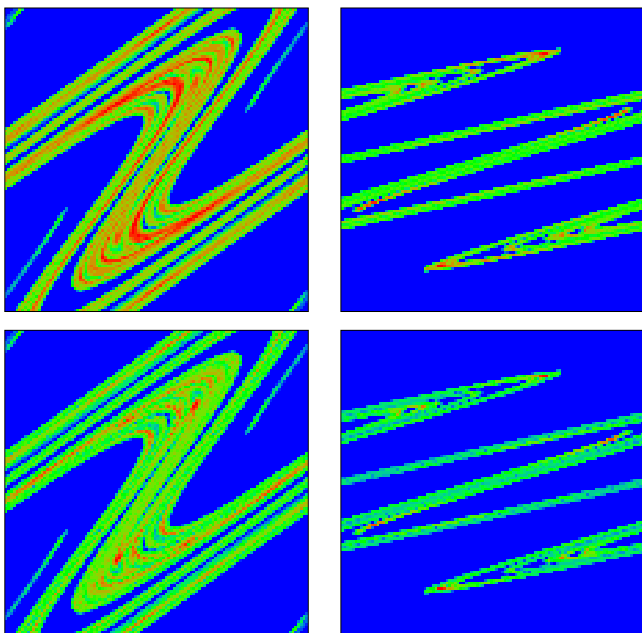
Fig. 1. (Color online) Phase space representation of eigenstates ψ_i of the Ulam matrix approximant **S** of the Perron-Frobenius operator for models 1 and 2 at $N = 110 \times 110$ (color is proportional to $|\psi_i|$ with red/gray for maximum and blue/black for zero). Left column shows eigenstates for the model 1 at $K = 7, a = 2$ for maximum $\lambda_1 = 0.756$ (top panel) and $\lambda_3 = -0.01 + \imath 0.513$ (bottom panel), the space region is $(-aK/2 \leq y \leq aK/2, 0 \leq x \leq 2\pi)$ and the fractal dimension of the strange repeller is $d = 1.769$. Right column shows eigenstates for the model 2 at $K = 7, \eta = 0.3$ for maximum $\lambda = 1$ (top panel) and $\lambda_3 = -0.258 + \imath 0.445$ (bottom panel), the space region is $(-4\pi \leq y \leq 4\pi, 0 \leq x \leq 2\pi)$ and the fractal dimension of the strange attractor is $d = 1.532$.

pared to dynamical chaos and thus , in the limit of small cell size, the physical properties of the dynamics are expected to have no significant modifications in agreement with the results presented in [16,18]. Our numerical results obtained for dynamical maps with homogeneous chaotic dynamics confirm the convergence of the Ulam method to the continuous limit of the Perron-Frobenius operator.

The paper is organized in the following way: Section II gives the model description; Section III presents the numerical results and the discussion is given in Section IV.

2 Model description

To study the validity of the fractal Weyl law we use the Chirikov standard map [12]. We consider two models: the map with absorption that corresponds to the classical limit of the quantum model studied in [13,10] (model 1) and the map with dissipation (model 2) also known as the Zaslavsky map [20]. In the first model the dynamics

is described by the map

$$\begin{cases} \bar{y} = y + K\sin(x + y/2) \\ \bar{x} = x + (y + \bar{y})/2 \pmod{2\pi} \end{cases} \qquad (2)$$

where bar notes the new values of dynamical variables and K is the chaos parameter. The map is written in its symmetric form and all orbits going out of the interval $-aK/2 \leq y \leq aK/2$ are absorbed after one iteration. We consider a strong chaos regime at fixed $K = 7$ and vary the classical escape time by changing a in the interval $0.8 \leq a \leq 6$.

The second model is described by the map with dissipation parameter $\eta < 1$:

$$\begin{cases} \bar{y} = \eta y + K\sin x \\ \bar{x} = x + \bar{y} \pmod{2\pi} \end{cases} \qquad (3)$$

with periodic boundary conditions in $y \in [-4\pi, 4\pi)$. Due to dissipation and chaos the dynamics converges to a strange attractor (see e.g. [21]).

To construct the Ulam matrix approximant for a continuous Perron-Frobenius operator in the two-dimensional phase space we divide the space of dynamical variables (x, y) on $N = N_x \times N_y$ cells with $N_x = N_y$. Then N_c trajectories are propagated on one map iteration from a cell j, and the elements S_{ij} are taken to be equal to a relative number N_i of trajectories arrived at a cell i ($S_{ij} = N_i/N_c$ and $\sum_i S_{ij} = 1$). Thus the matrix **S** gives a coarse-grained approximation of the Perron-Frobenius operator for the dynamical map. The map gives about K links for each cell. We use N_c values from 10^4 to 10^6 where the results are independent of N_c. The fractal dimension d of the strange repeller and attractor depends on system parameters and is computed as a box counting dimension using standard methods [21].

We also used another method to construct the Ulam matrix based on a one trajectory for the dynamics with a strange attractor in the model 2. In the one trajectory Ulam method we iterate one trajectory up to time $t_1 = 100$; after that we continue iterations of the trajectory up to time $t = 10^9$ and determine the matrix elements S_{ij} as the ration between the number of transitions from cell j to cell i divided by the total number of transitions N_c from cell j to all other cells (in this way $\sum_i S_{ij} = 1$). This approach has certain advantages since it gives the Ulam matrix restricted to a dynamics only on the attractor. For a given cell size this method gives a significantly smaller matrix size $N_a \ll N$ since the number of cells N_a located on the attractor is much smaller than the total number of cells N. When speaking about the results based on the one trajectory Ulam method we always directly specify this.

3 Numerical results

The eigenvalues λ_i and right eigenvectors ψ_i of the matrix **S** ($\mathbf{S}\psi_i = \lambda_i\psi_i$) are obtained by a direct diagonalization. Examples of the eigenstates with maximal absolute values of λ_i are shown in Fig.1. The fractal structure of eigenstates is evident. For the model 1 the measure is decreasing
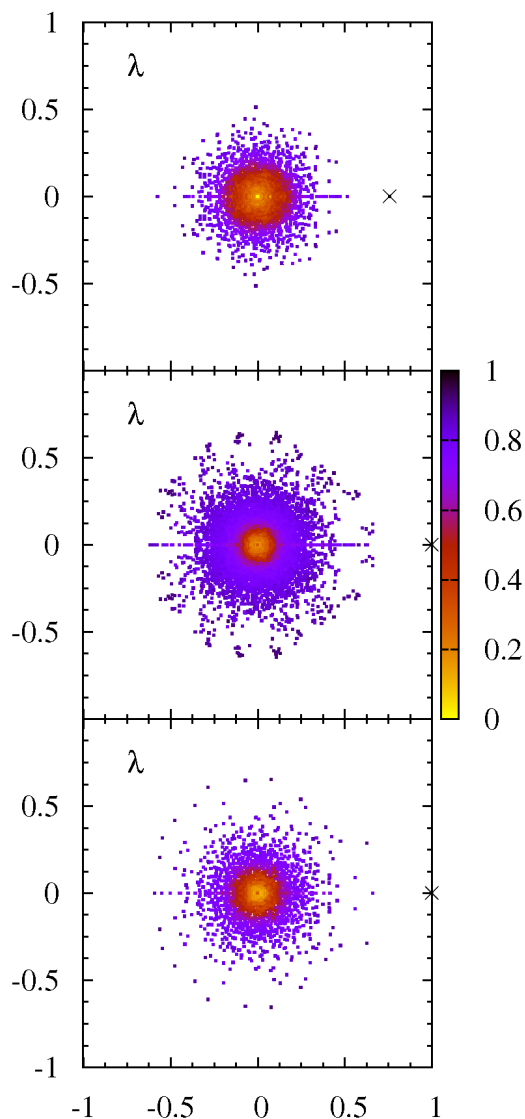
Fig. 2. (Color online) Distribution of eigenvalues λ in the complex plane for the Ulam matrix approximant **S** for the parameters of Fig.1 for the models 1 (top panel) and 2 (center panel). Bottom panel shows the spectrum for the model 2, with the same parameters as for the central panel, obtained via the one trajectory Ulam approximant (see text). Color/grayness of small squares is determined by the value of overlap measure μ defined in the text and shown in the palette.

due to absorption and $\lambda_1 < 1$, the state with λ_1 represents a set of strange repeller formed by orbits nonescaping in future. For the model 2 all measure drops on the strange attractor and in agreement with the Perron-Frobenius theorem we have $\lambda = 1$ [15]. Other eigenstates with smaller values of $|\lambda|$ are located on the same fractal set as the states with maximal λ_1 but have another density distribution on it.

The spectrum of matrix **S** in the complex plane is shown in Fig.2. It has a maximal real value λ_1 isolated

by a gap from a cloud of eigenvalues more or less homogeneously distributed in a circle of radius r_λ. For the model 2 the dense part of the spectrum has $r_\lambda \approx \eta$ (at least at small values of η) that physically corresponds to the fact that η gives the relaxation rate to the limiting set of the strange attractor. The gap between λ_1 and other eigenvalues in the model 1 is probably related to a dynamics on the strange repeller. According to [10] the decay rate of total probability in (2) is exponential in time with the rate $\gamma_c = 0.270$ (for parameters of Figs.1,2). This agrees well with the numerical value $\lambda_1 = 0.756 \approx \exp(-\gamma_c)$. The data of Fig.1 indicate that the states with $i > 1$ have a strong overlap with the steady state of λ_1 ($i = 1$). In a quantitative way this overlap can be characterized by an overlap measure defined as $\mu_i = \sum_l \psi_1(l)|\psi_i(l)|$ where the sum runs over all N cells. For μ close to unity an eigenstate ψ_i has a strong overlap with the steady state ψ_1 and such states can be viewed as higher mode excitations on this domain. For $\mu \ll 1$ we have other type of states being rather different from ψ_1. The data of Fig.2 show that states with small values of $|\lambda|$ have small μ.
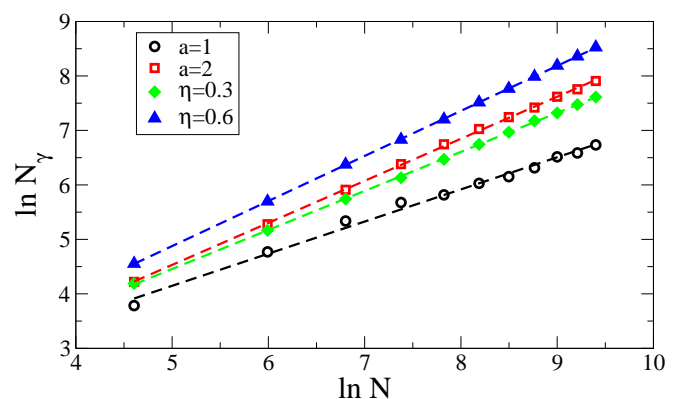
Fig. 3. (Color online) Dependence of the integrated number of states N_γ with decay rates $\gamma \leq \gamma_b = 16$ on the size N of the Ulam matrix **S** for the models 1 and 2 at $K = 7$. The fits of numerical data, shown by dashed straight lines, give $\nu = 0.590, d = 1.643$ (at $a = 1$); $\nu = 0.772, d = 1.769$ (at $a = 2$); $\nu = 0.716, d = 1.532$ (at $\eta = 0.3$); $\nu = 0.827, d = 1.723$ (at $\eta = 0.6$).

In fact, as it is typical of the fractal Weyl law, almost all eigenvalues drop to very small $|\lambda| \to 0$. The number of states within a finite band with $0 \leq \gamma \leq \gamma_b$, where $|\lambda| = \exp(-\gamma/2)$, grows algebraically with N with the exponent $\nu < 1$ remaining small compared to N. Typical examples of such a dependence are shown in Fig.3 for both models.

The spectrum for the one trajectory Ulam approximant is shown in the bottom panel of Fig.2 (here $N_a = 2308$ while $N = 12100$). The spectrum with one trajectory has a structure similar to the spectrum of the usual Ulam method. This shows that the spectrum is mainly determined by the diffusive type excitations on the attractor.
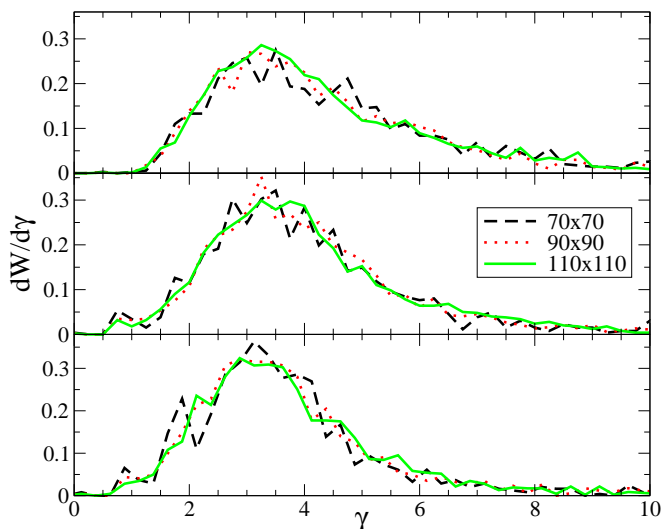
Fig. 4. (Color online) Dependence of density of states $dW/d\gamma$ on the decay rate γ for the Ulam matrix $\mathbf{S}$ for the model 1 (top panel), and model 2 (center panel) at different sizes $N = N_x \times N_y$ given in the inset. Bottom panel shows the spectral density for the one trajectory Ulam method for parameters of the central panel. Data are shown for parameters of Fig.1, the density is normalized by the condition $\int_0^{16} dW/d\gamma \, d\gamma = 1$.

Our matrix sizes N are sufficiently large and allow to reach asymptotic behavior in the limit of large N. This is confirmed by the fact that the density of states $dW/d\gamma$ in γ becomes independent of N as it is show in Fig. 4. This directly demonstrates that the Ulam method is stable for our models and that it converges to the continuous limit of the Perron-Frobenius operator. The density of states for the Ulam matrix obtained with one trajectory has the density of states very close to the one obtained by the usual Ulam method. This shows that the spectrum with finite values of γ is determined by the dynamics on the attractor.

The density is mainly determined by the cloud of states in the radius r_λ, the contribution of the isolated eigenvalue λ_1 is only weakly visible at minimal γ. The density has a broad maximum around $\gamma \approx 3$, for the model 2 this value is compatible with the value $-2\ln\eta$ which determines the global relaxation rate to the strange attractor. It is interesting to note that for the model 1 the spectral density of the Perron-Frobenius operator (Fig.4, top panel) is rather different from the spectral density in the corresponding quantum problem (Fig.4 in [10]). Indeed, the densities $dW/d\gamma$ for the classical and quantum systems are very different: the classical model 1 has one isolated eigenvalue λ_1 and a broad maximum around $\gamma \approx 3$. The quantum model of [10] has a peaked distribution around $\gamma_c = -2\ln\lambda_1$ corresponding to the classical state at λ_1 and a monotonically decreasing density at larger values of γ. At the same time the eigenstates with minimal γ are located on the strange set of trajectories nonescaping in future times, both in the classical and quantum cases (see

Fig.1 here and in [10]). Thus the semiclassical correspondence between classical and quantum cases of model 1 still requires a better understanding.
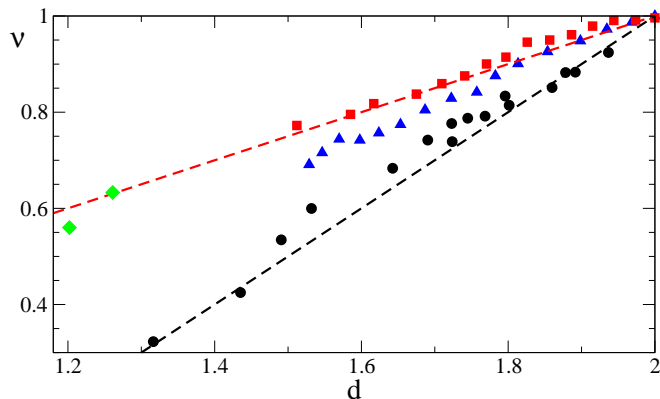
Fig. 5. (Color online) Fractal Weyl law for three different models: models 1 (black points at $K = 7$) and 2 (red/gray squares at $K = 12$, blue/black triangles at $K = 7$) and Hénon map (green/gray diamonds at $a = 1.2; 1.4$ for $b = 0.3$). The fractal Weyl law exponent ν is shown as a function of fractal dimension d of the strange forward trapped set in model 1 and strange attractor in model 2 and Henon map. The straight dashed lines show the laws (4) (upper line) and (1) (bottom line). We used $a \in [0.8, 6]$ for model 1 and $\eta \in [0.3, 1]$ for model 2.

We determine the exponent ν as it is shown in Fig. 3 for both models at different values of parameters. At the same time we compute the fractal dimension d of the strange set of trajectories nonescaping in future using box counting dimension with a box size ϵ. In this way the size of the Ulam matrix is $N = 1/\epsilon^2$ while the number of cells on the fractal set scales as $N_f \propto 1/\epsilon^d = N^{d/2}$. In this way we determine the dependence of ν on d. The data are shown in Fig. 5. For the model 1 we find that the usual fractal Weyl law with $\nu = d - 1$ holds in a large interval of variation of d. Relatively small deviations can be attributed to a finite accuracy in computation of ν at finite matrix sizes. In contrast to that for the model 2 we find absolutely another relation which can be approximately described as

$$N_\gamma \propto N^\nu \ , \ \ \nu = d/2 \ . \tag{4}$$

This relation works rather well for $K = 12$ while for $K = 7$ the deviations are a bit larger. We attribute this to the fact that at $K = 7$ there is a small island of stability at $\eta = 1$ [22] which does not influence the dynamics in the case of absorption (2) but can produce certain influence for the dissipative case (3). To check that the law (4) works for other systems with strange attractors we computed ν and d for the Hénon map ($\bar{x} = y + 1 - ax^2, \bar{y} = bx$, see e.g. [21]) at standard parameter values of a, b. The results confirm the validity of the fractal Weyl law also for the Hénon map (see Fig. 5).

The physical origin of the law (4) can be understood in a simple way: the number of states N_γ with finite values

of γ is proportional to the number of cells $N_f \propto N^{d/2}$ on the fractal set of strange attractor. Indeed, the results for the overlap measure μ (see Fig. 2) show that these states have strong overlap with the steady state while the states with $\lambda \to 0$ have very small overlap. Thus almost all N states have eigenvalues $\lambda \to 0$ and only a small fraction of states on the strange attractor $N_\gamma \propto N_f \propto N^{d/2} \ll N$ has finite values of λ. We also checked that the participation ratio ξ of the eigenstate of model 2 at $\lambda = 1$, defined as $\xi = (\sum_l |\psi_1(l)|^2)^2 / \sum_l |\psi_1(l)|^4$, grows as $\xi \sim N_f \propto N^{d/2}$.

The fractal Weyl laws (1) and (4) have two different exponents ν but they correspond to two different situations: for (1) the law describes the systems with absorption when all measure escapes from the system and only a small fractal set remains inside; for (4) all measure drops on a fractal set inside the system. Due to that reasons the exponents are different.
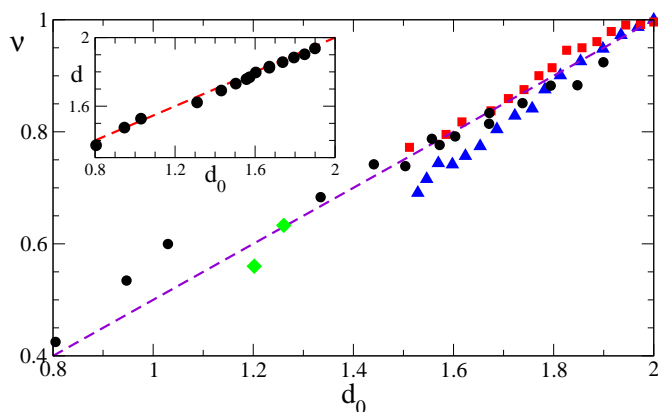
Fig. 6. (Color online) Fractal Weyl law for three different models as a function of the dimension of the invariant set d_0; the models and their parameters are the same as in Fig. 5. The fractal Weyl exponent ν is shown as a function of fractal dimension d_0 of the strange repeller in model 1 and strange attractor in model 2 and Henon map. The straight dashed line show the theoretical dependence $\nu = d_0/2$ of Eq. (5). The inset shows the relation between the fractal dimension d of trajectories nonescaping in future and the fractal repeller dimension d_0 for the case of model 1; the dashed straight line shows the theoretical dependence $d = d_0/2 + 1$.

The different dependencies of ν on d in Eqs. (1,4) can be reduced to one dependence if to express ν via the fractal dimension d_0 of the invariant sets. Indeed, for the model (2) all trajectories drop on the strange attractor which can be considered as an invariant set with the fractal dimension $d_0 = d$. For the model 1 we have the set of trajectories nonescaping in future with dimension d, there is also the fractal set of trajectories nonescaping in the past which has also the dimension d due to symmetry between the future and the past present in the model 1 (symmetry to reflection $x, y \to -x, -y$ in (2)). Then the invariant set of a strange repeller corresponds to the intersection of these

two sets of trajectories nonescaping neither in the future neither in the past with the fractal dimension d_0. As it is known, see e.g. [21], we have $2 = d + d - d_0$ so that $d = d_0/2 + 1$. This relation is confirmed by the data presented in the inset of Fig. 6. On the basis of these relations we can express the fractal Weyl exponent via the fractal dimension d_0 of the invariant set

$$N_\gamma \propto N^\nu , \quad \nu = d_0/2 . \tag{5}$$

This global dependence is confirmed by the data shown in Fig. 6.

The numerical data for the one trajectory Ulam method gives always $N_\gamma \propto N_a$. This satisfies the relation (5) since by definition $N_a \propto N^{d_0/2}$.

4 Discussion

In summary, our results show that the Ulam method gives very efficient possibility to study the spectral properties of the Perron-Frobenius operators for systems with dynamical chaos. Their spectrum is characterized by the fractal Weyl law with the Wyel exponent determined by the fractal dimension of dynamical system according to relations (1), valid for systems with absorption or chaotic scattering, or (4), valid for dissipative systems with strange attractors.

It is interesting to note that for dynamical systems the Ulam method naturally generates directed Ulam networks [18] which have certain similarities with the properties of the Google matrix of the World Wide Web (WWW). However, for the model 2 and the Hénon map considered above, there is a finite gap between $\lambda = 1$ and other eigenvalues while for the WWW there is no such gap [23,24]. In this sense the above models are more close to randomized directed networks considered in [25] which have a relatively large gap. We note that the PageRank vector ψ_1 with $\lambda = 1$, used by Google for ranking of web pages, corresponds in our case to a strange attractor. In this case the probability $p_l \sim \psi_1(l)$ is distributed over all cells $N_f \propto N^{d/2}$ occupied by the strange attractor. The number of such cells grows infinitely with N that corresponds to a delocalized phase of the PageRank similar to the cases discussed in [18]. In contrast to that the WWW is characterized by a localized PageRank with an effective finite number of populated sites independent of N. In spite of that it is not excluded that the future evolution of the WWW can enter in a delocalized regime of the PageRank. Therefore, we think that the fractal Weyl law discussed here can be useful not only for the Perron-Frobenius operators of dynamical systems but also for various types of realistic directed networks.

References

1. H. Weyl, Math. Ann. **141**, 441 (1912).
2. G. A. Gamow, Z. für Phys. **51**, 204 (1928).
3. N. Moiseyev, Phys. Rep. **208**, 211 (1998).

4. P. Gaspard, *Chaos, Scattering and Statistical Mechanics*, Cambridge Univ. Press, Cambridge (1998).

5. C. Gmachl, F. Capasso, E.E. Narimanov, J.U. Nöckel, A.D. Stone, J. Faist, D.L. Sivco and A. Y. Cho, Science **280**, 1556 (1998).

6. J. Sjöstrand, Duke Math. J. **60**, 1 (1990); M. Zworski, Not. Am. Math. Soc. **46**, 319 (1999); J. Sjöstrand and M. Zworski, Duke Math. J. **137**, 381 (2007); S. Nonnenmacher and M. Zworski, Commun. Math. Phys. **269**, 311 (2007).

7. W. T. Lu, S. Sridhar and M. Zworski, Phys. Rev. Lett. **91**, 154101 (2003).

8. H. Schomerus and J. Tworzydlo, Phys. Rev. Lett. **93**, 154102 (2004).

9. J.P. Keating, M. Novaes, S.D. Prado and M. Sieber, Phys. Rev. Lett. **97**, 150406 (2006); S. Nonnenmacher and M. Rubin, Nonlinearity **20**, 1387 (2007).

10. D.L. Shepelyansky, Phys. Rev. E **77**, 015202(R) (2008).

11. L. Ermann, G.G. Carlo, and M. Saraceno, Phys. Rev. Lett. **103**, 054102 (2009); J.M. Pedrosa, G.G. Carlo, D.A. Wisniacki and L. Ermann, Phys. Rev. E **79**, 016215 (2009).

12. B. V. Chirikov, Phys. Rep. **52**, 263 (1979); B.Chirikov and D.Shepelyansky, Scholarpedia, **3**(3): 3550 (2008).

13. F. Borgonovi, I. Guarneri and D.L. Shepelyansky, Phys. Rev. A **43**, 4517 (1991); G. Casati, G. Maspero and D.L. Shepelyansky, Physica D **131**, 311 (1999).

14. S.M. Ulam, *A Collection of mathematical problems*, Vol. 8 of Interscience tracs in pure and applied mathematics, Interscience, New York, p. 73 (1960).

15. M. Brin and G. Stuck, *Introduction to dynamical systems*, Cambridge Univ. Press, Cambridge, UK (2002).

16. T.-Y. Li, J. Approx. Theory **17**, 177 (1976); M. Blank, G. Keller, and C. Liverani, Nonlinearity **15**, 1905 (2002); D. Terhesiu and G. Froyland, Nonlinearity **21**, 1953 (2008).

17. Z. Kovács and T. Tél, Phys. Rev. A **40**, 4641 (1989); G. Froyland, R. Murray and D. Terhesiu, Phys. Rev. E **76**, 036702 (2007).

18. D.L. Shepelyansky and O.V. Zhirov, arXiv:0905.4162v2[cs.IR] (2009).

19. L. Guillopé, K.K. Lin, and M. Zworski, Commun. Math. Phys. **245**, 149 (2004).

20. G.M. Zaslavsky, Phys. Lett. A **69**, 145 (1978); Scholarpedia, **2**(5): 2662 (2007).

21. E. Ott, *Chaos in Dynamical Systems*, Cambridge Univ. Press, Cambridge (1993).

22. B.V. Chirikov, arXiv:nlin/0006013 (2000).

23. S. Brin and L. Page, Computer Networks and ISDN Systems **33**, 107 (1998).

24. A. M. Langville and C. D. Meyer, *Google's PageRank and Beyond: The Science of Search Engine Rankings*, Princeton University Press (Princeton, 2006).

25. O. Giraud, B. Georgeot and D. L. Shepelyansky, Phys. Rev. E **80**, 026107 (2009).